Available online at www.sciencedirect.com
ScienceDirect
Ultrasonics Sonochemistry 14 (2007) 456–469
Ultrasonics SONOCHEMISTRY
www.elsevier.com/locate/ultsonch

Numerical simulations of the aspherical collapse of laser and acoustically generated bubbles

Kostas Tsiglifis, Nikos A. Pelekasis *

Department of Mechanical and Industrial Engineering, University of Thessaly, Volos 38334, Greece

Received 23 July 2006; accepted 30 October 2006
Available online 8 January 2007

Abstract

The details of nonlinear axisymmetric oscillations and collapse of bubbles subject to large internal or external pressure disturbances, are studied via a boundary integral method. Weak viscous effects on the liquid side are accounted for by integrating the equations of motion across the boundary layer that is formed adjacent to the interface. Simulations of single-cavitation bubble luminescence (SCBL) and single-bubble sonoluminescence (SBSL) are performed under conditions similar to reported experimental observations, aiming at capturing the details of bubble collapse. It is shown that any small initial deviation from sphericity, modeled through a small initial elongation along the axis of symmetry, may result in the formation and impact of two counter-propagating jets during collapse of the bubble, provided the amplitude of the initial disturbance is large enough and the viscosity of the surrounding fluid is small enough. Comparison between simulations and experimental observations show that this is the case for bubbles induced via a nano-second laser pulse (SCBL) during a luminescence event. In a similar fashion, simulations show that loss of sphericity accompanied with jet formation and impact during collapse is also possible with acoustically trapped bubbles in a standing pressure wave (SBSL), due to the many afterbounces of the bubble during its collapse phase. In both cases jet impact occurs as a result of P_2 growth in the form of an afterbounce instability. When the sound amplitude is decreased or liquid viscosity is increased the intensity of the afterbounce is decreased and jet impact is suppressed. When the sound amplitude is increased jet formation is superceded by Rayleigh–Taylor instability. In the same context stable luminescence is quenched in experimental observations. In both SCBL and SBSL simulations the severity of jet impact during collapse is quite large, and its local nature quite distinct. This attests to the fact that it is an energy focusing mechanism whose importance in generating the conditions under which a luminescence event is observed should be further investigated.

PACS: 4325.+y; 78.60.Mq; 47.11+j; 47.27Wg; 47.55dz

Keywords: Nonlinear acoustics; Sonoluminescence; Computational methods in fluid dynamics; Jets; Bubble dynamics; Weak viscous effects; Collapse; Laser bubbles

1. Introduction

In the past decade a large number of studies have been aimed at elucidating the mechanism that explains the mechanical action of a collapsing bubble, when light emission is observed during cavitation. One of the earlier proposed mechanisms assumes the generation of a converging shock wave upon bubble collapse [1], giving rise to a hot spot and to the generation of partly ionized plasma in the bubble center [2,3]. This would imply a certain degree of sphericity of the collapse as a necessary prerequisite for light emission. Indeed, recent experimental techniques based on high-speed photographic or holographic methods [4] have revealed, using acoustically (single bubble sono luminescence) and laser induced bubbles (single cavitation bubble luminescence), that there is a threshold of asphericity below which luminescence occurs. In fact, it was seen that shock-wave emission is not necessarily

* Corresponding author. Tel.: +30 24210 74102; fax: +30 24210 74050.
E-mail addresses: kotsigl@uth.gr (K. Tsiglifis), pel@uth.gr (N.A. Pelekasis).

1350-4177/$ - see front matter © 2006 Elsevier B.V. All rights reserved.
doi:10.1016/j.ultsonch.2006.10.009

connected with a luminescence event in cases for which collapse was not violent enough, as for example in the presence of a nearby solid boundary. Recent experimental results [5] with laser induced bubbles allowing for better control of bubble size and level of initial asphericity, corroborate the importance of sphericity. Bubbles produced via a nano-second laser pulse tend to be of almost spherical initial shape and relatively large, initial radius, R_0, on the order of 0.5 mm, and consequently collapse in a violent fashion with significant light emission. Those obtained via a femto-second laser pulse are smaller, initial radius on the same order as acoustically trapped bubbles, 5 μm, but with significant elongation. Such bubbles were observed to collapse aspherically without any detectable light emission.

On the other hand there are theories [6,7] that assert that even when the bubble shape is initially very close to spherical, asymmetric collapse happens at the last stages giving rise to jet formation and impact. Simulations of bubbles translating with a traveling wave exhibit jet formation upon collapse, accompanied by the appearance of toroidal bubbles [8,9]. The experiments that have been performed on SBSL cannot clearly capture the pattern that prevails at the final stages, due to the enormous velocity of the bubble interface as well as to the extremely small bubble size during the final collapse stage. Furthermore, in SBSL studies bubbles are typically trapped in a standing wave, in which case their translational velocity is close to zero. However, it is still present due to small variations in the primary Bjerknes force and this is expected to generate very small disturbances in the bubble shape. Nevertheless, it is believed [6] that, irrespective of the more or less spherical nature of bubble pulsations, sphericity may be lost during the very last stages of collapse and this conjecture is supported by experimental investigations [10,11] indicating that sonoluminescence occurs within a parameter range, in terms of bubble size and sound amplitude, that is adjacent to that corresponding to shape instabilities. This general pattern is reproduced in experiments with bubbles induced via a nano-second laser pulse [5], where a nearly spherosymmetric collapse is accompanied by light emission and a detectable loss of spherosymmetry at the time instant of minimum volume slightly before rebound takes place, Fig. 1a. In order to clarify the details of collapse, simulations of laser and acoustically induced bubbles are necessary in a parameter range where light emission is observed. This will help us assess the influence of bubble size, sound amplitude, liquid viscosity and nonuniformities in the initial bubble shape on jet formation and impact in cases for which a net translational velocity of the bubble is not present, as for example when bubbles are trapped via a standing pressure wave or induced via a laser pulse.

At this point, it should be stressed that in the literature of sonoluminescence and as far as acoustically trapped bubbles are concerned, the most widely accepted mechanism behind light emission is that of adiabatic collapse [12,13]. According to this mechanism the collapse phase

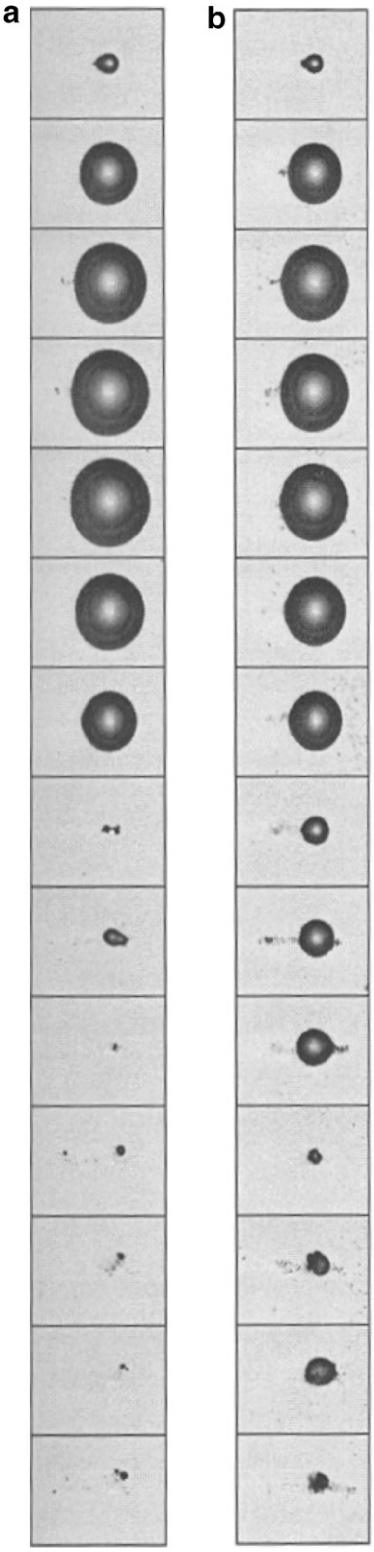

Fig. 1. (a) Frame sequence depicting the collapse of a bubble generated via a nano-second laser pulse. The host liquid is water at normal pressure and temperature conditions. The width of each frame corresponds to 4 mm. The first frame is captured at $t'_1 = 2$ μs while subsequent frames are captured at a time interval of 30 μs. The laser pulse is applied from the left and imparts 3.8(4) mJ to the host liquid. (b) Frame sequence obtained in the same fashion as in (a) with the difference that the host fluid is a 5% water solution of acetone at the same temperature and pressure conditions. All the above figures are reproduced from [5].

of the bubble occurs in a more or less adiabatic fashion. Thus, the larger the reduction in the bubble volume from its maximum to its minimum radius the larger the accompanying temperature rise inside the bubble, and this generates the necessary conditions for ionization of the gas inside the bubble and subsequent light emission. In addition, phase diagrams obtained based on shape and diffusion stability requirements [14,15] predict a stability range that is close to that obtained from experiments with stably luminating bubbles [11]. In this fashion neither a shock wave nor jet impact are necessary for explaining light emission. However, there are still some remaining issues to be addressed such as the quenching of light emission with increasing viscosity of the surrounding fluid [16]. Recent studies [17] attribute this effect to the inability to trap bubbles in a stable position inside a viscous fluid, and the establishment of a 3d trajectory. In the present study we will try to assess the effect of increased liquid viscosity on the bubble collapse pattern and the resulting asymmetry during collapse.

It is not in the scope of the present study to assess the relative merits of the above mentioned mechanisms. Rather, it is intended at detecting the pattern of bubble collapse as well as details of the flow arrangement, under different external conditions and fluid properties. In addition, calculations of the interfacial and jet velocities during collapse may enlighten their relative importance in luminescence, even if the present model cannot simulate the generated shock wave and does not take into account dissipation due to compressibility. The latter is expected to stabilize shape instabilities and raise the threshold in sound amplitude for the appearance of the Rayleigh–Taylor instability in collapsing bubbles [18]. It is also interesting to correlate the appearance of shape instabilities, as predicted asymptotically [14,15,18,19] for acoustically levitated bubbles, with shape deformation and break-up as predicted numerically when the assumption of spherosymmetry is relaxed and the effect of viscous dissipation inside the boundary layer surrounding the bubble is taken into account. To this end, a hybrid boundary-finite element method is used in order to solve for the velocity potential and shape deformation of axisymmetric bubbles. Weak viscous effects are included in the computations by retaining first-order viscous terms in the normal stress boundary condition and satisfying the tangential stress balance. Details on the model equations and assumptions as well as the numerical methodology and the relevant dimensionless parameters, have been given elsewhere [20].

In Section 2, a brief account is given of the special features of SCBL and simulations are presented of specific experimental observations, where light emission is observed in pure water. Moreover, simulations of SCBL in water–acetone solution are performed, in which case no light is observed. The effect of initial asymmetries in the bubble shape on the final collapse mode is also analyzed, performing simulations of SCBL with varying initial elongation. Finally, calculations of jet and interfacial velocities are shown for each case. In Section 3, SBSL is studied and results of simulations are shown, obtained in conditions similar with experiments where luminescence takes place. The pattern of shape deformation, interfacial vs. Rayleigh–Taylor instability, and collapse is captured and the evolution of the interfacial and jet velocities during the last stages of collapse are calculated and compared. Finally, in Section 4 the relative importance of different parameters on the details of bubble collapse is emphasized, e.g. degree of sphericity during collapse and jet formation as a function of sound amplitude, liquid viscosity, bubble size and level of initial asymmetry, and conclusions are drawn.

2. Simulation of single-cavitation bubble luminescence (SCBL)

In single-cavitation bubble luminescence a laser pulse with duration on the order of a few femto- or nano-seconds [5] causes heating of impurities and/or dielectric breakdown with avalanche ionization, thus creating a plasma spot. The plasma recombines to generate a gas and vapor filled bubble. The biggest part of the initial energy due to the laser pulse is consumed in order to locally form plasma. Energy is also dissipated in the form of thermal and acoustic energy of the host fluid, and only a small part, roughly 10%, is converted to mechanical energy of the bubble which can then be quantified in terms of the internal overpressure when the bubble starts expanding at $t = 0$. After the instant of bubble inception and within a very short period of time, part of the liquid vapor cools down and re-condenses. It is assumed that this process is completed within the time interval $0 < t < t_1$, t_1 is the time needed to capture the first frame depicting the shape of the bubble and is on the order of a few microseconds for nano-second bubbles and a few hundreds of nano-seconds for femto-second bubbles. From this point onwards the bubble expands and collapses in a more or less isothermal fashion, except for the very last moments of collapse in which case large pressures and temperatures are generated. After the point of collapse the bubble rebounds and eventually settles to its equilibrium radius, R_{Eq}, as can be seen in Fig. 1a. As mentioned above, femto-seconds bubbles have large initial elongations and their initial radius is on the order of 5 μm, while nano-seconds bubbles acquire an almost spherical initial shape and their initial size is on the order of 400 μm. Bubbles of the latter size are seen to emit light at collapse and consequently our simulations are aimed at capturing the details of their collapse while conforming to experimental observations.

The equivalent radius R_0 of the bubble at $t = 0$ is assigned as the characteristic length of the problem. It is determined based on the known initial bubble volume. In the absence of a characteristic velocity, surface tension is used in order to render velocity, pressure and time dimensionless. The dimensionless parameters that determine the

dynamics of the problem are the amplitude of the disturbance of internal pressure ε_B, the dimensionless static pressure at infinity P_{St}, the initial bubble elongation S and the Reynolds number Re of the external liquid. The initial shape of the bubble is taken to be that of an axisymmetric ellipsoid with two semi-axes of equal length, $a = b$. The extent of initial elongation is measured by the ratio $S = a/R_0$, while the length of the third semi-axis, c, corresponding to the axis of symmetry is recovered as $c/R_0 = 1/S^2$. As S deviates from unity, i.e. a perfectly spherical shape, the shape becomes oblate, $S > 1$, or prolate, $S < 1$. The latter corresponds to an elongation along the axis of symmetry that is intensified as S is further decreased. In the following the XY plane denotes a projection of the bubble shape on a specific meridian with X signifying the axis of symmetry. More details are provided in Ref. [20].

In Fig. 1a and b two sequences of frames of nano-second laser bubbles, recorded experimentally with pure water and a 5% water solution of acetone as host fluids, respectively, are presented. In an effort to account for the complicated processes of mass and heat transfer that take place during the early stages of bubble inception, $0 < t < t_1$, in a simplified manner, we obtain estimates of the parameters that affect bubble dynamics based on the above mentioned sequence of interfacial shapes. First the equilibrium radius is estimated from the last frame corresponding to bubble equilibrium. Then, for given conditions in the quiescent fluid the internal bubble pressure is estimated and consequently, employing the isothermal ideal gas law, the pressure inside the bubble at $t = t_1$ can be calculated, $P_G(t = t_1)$, because its volume is also known at this time instant. However, this is not the original bubble overpressure, $P_G(t = 0_+) = (1 + \varepsilon_B)(P_{St} + 1)$, since condensation has already taken place before $t = t_1$. It should be added that the simulation cannot start at $t = t_1$ since the kinetic energy of the bubble is not known at that time. As a result the original overpressure at $t = 0$, $P_G(t = 0_+)$ is estimated by fitting the maximum bubble volume, V_{max}, as obtained from the available frame sequence. The simulation proceeds until $t = t_1$ at which point the pressure has to abruptly drop at the value $P_G(t = t_1)$ estimated based on the equilibrium conditions. This is just a simple way to account for re-condensation of liquid vapor. It is not expected to be far from reality for a host liquid like water that does not exhibit excessive evaporation. From this point on the simulation continues, with given internal bubble pressure, shape and kinetic energy, until the point of collapse. It is also important to note that even for an overall spherical collapse a small amount of initial elongation is always present. More details on the above simulation scheme can be found in [21].

In both cases depicted in Fig. 1a and b the bubble equivalent radius, as obtained from the initial volume, is roughly 0.42 mm and the bubbles collapse in a more or less spherosymmetric fashion. However, collapse in the first case is much more severe than in the second one and is

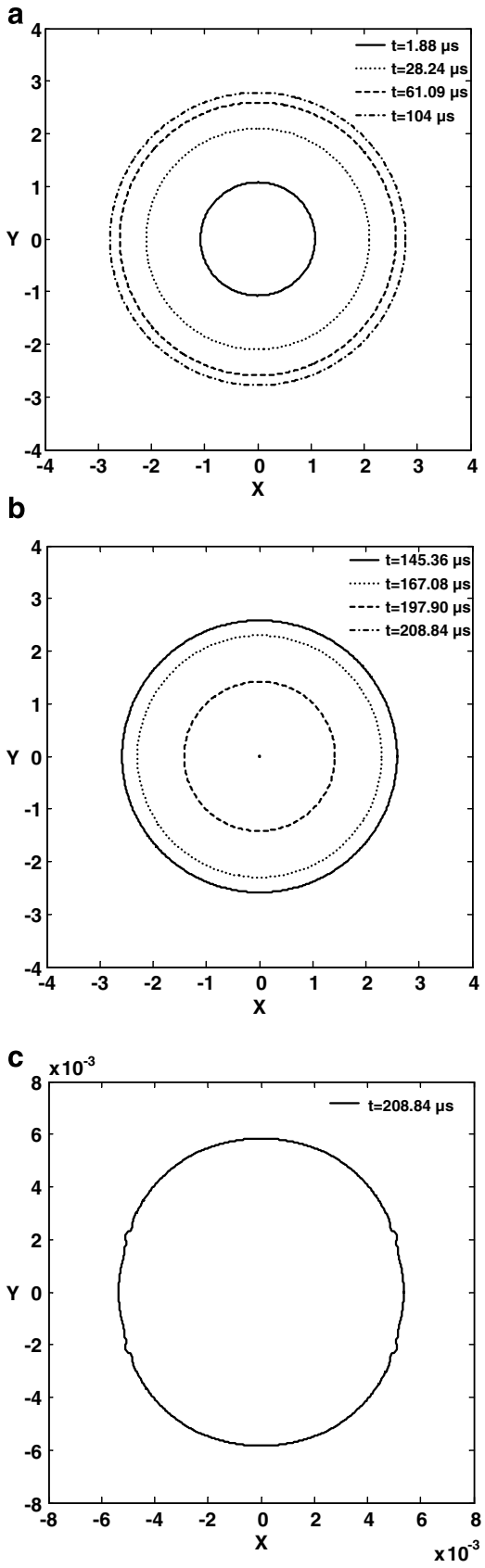

Fig. 2. Simulations of shape oscillations of nano-second laser bubbles in water, (a) during bubble expansion, (b) during bubble contraction and (c) at collapse; $S = 1$, $P_{St} = 295$, $\varepsilon_B = 81$, $Re = 174$, $P_G(t = 0) = 24400$, $P_G(t = t_1) = 298$.

characterized by significant photon emission. This is an interesting result since the thermophysical properties of these two substances are not very different, with the exception of vapor pressure that is much higher in the case of water and consequently acetone evaporates much easier. Simulating the case of pure water following the above algorithm and considering an initially spherical bubble shape ($S = 1$) we obtain the sequence of bubble shapes shown in Fig. 2. Clearly the minimum bubble volume at collapse, Fig. 2c, is much smaller than the one captured experimentally, frame # 8 in Fig. 1a, indicating an unrealistically violent collapse. In addition the bubble shape at collapse is more or less spherosymmetric, with the exception of areas with very small radius of curvature, while no jets are present. The interfacial velocity of the bubble at the point of collapse is calculated to, roughly, 80 000 m/s. It corresponds to the speed of the interface while it remains more or less spherosymmetric.

If the simulation is repeated with a very small initial elongation along the axis of symmetry ($S = 0.98$) the sequence of bubble shapes shown in Fig. 3 is obtained. In this case the bubble volume during the collapse phase, Fig. 3c, is closer to experimental observations. Careful observation of Fig. 1a and b shows that there is always a small deviation from sphericity at the early stages of bubble inception. This is intensified during the final stages of collapse through the formation of two microjets that move along the equatorial plane and coalesce at the axis of symmetry X, Fig. 3c. Fig. 3c belongs to a time interval around the time instant at which the frame depicting the minimum volume in Fig. 1a was captured, frame # 8 in Fig. 1a, and seems to exhibit remarkable agreement with the details of the latter. Plotting the mode decomposition of the bubble shape as a function of time, Fig. 4a and b, jet formation is identified as a result of an afterbounce instability dominated by the second Legendre mode, P_2, [15]. The strong

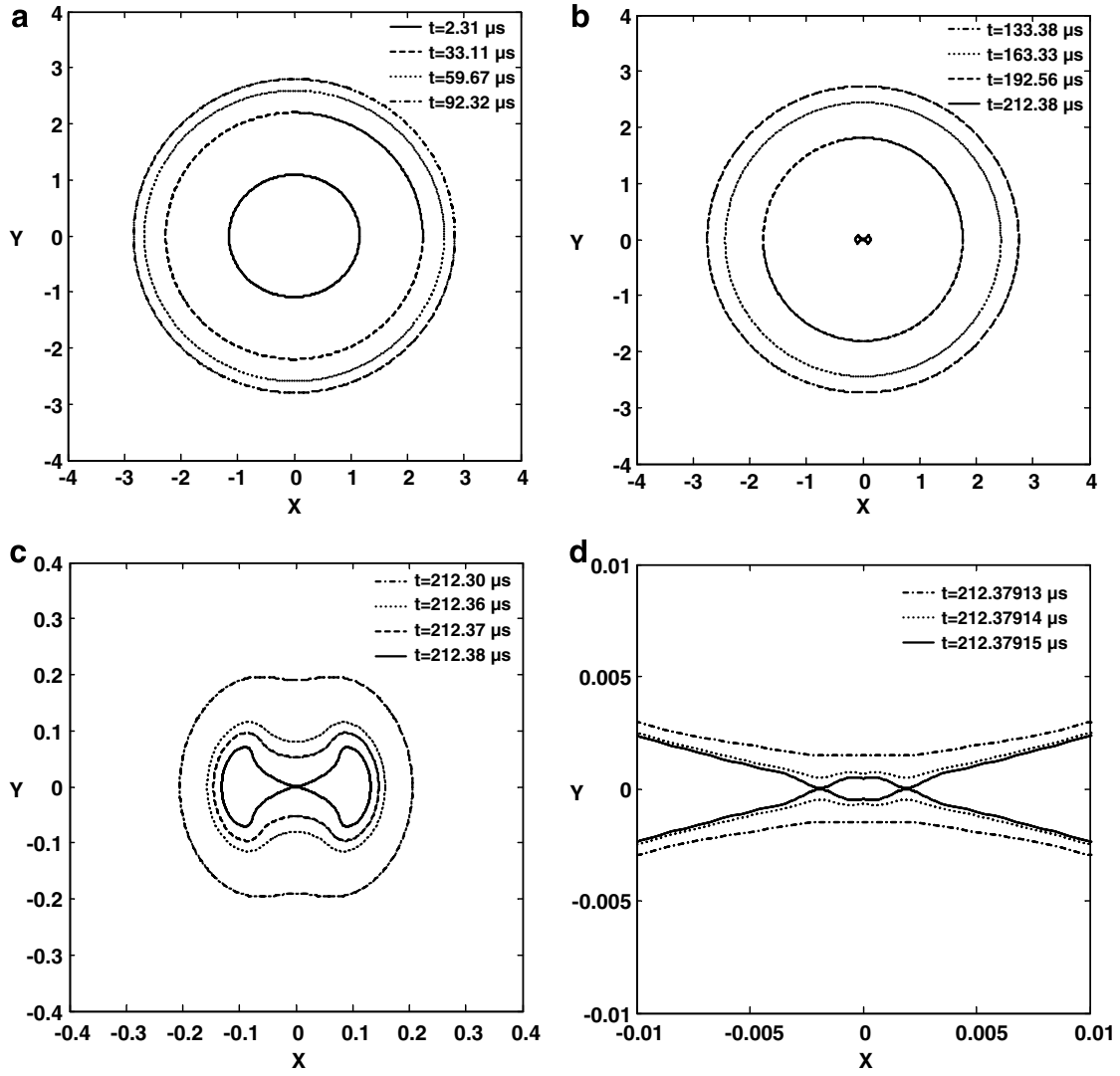

Fig. 3. Simulations of shape oscillations of nano-second laser bubbles in water, (a) during bubble expansion, (b) during bubble contraction, (c) during collapse and (d) focusing on jet impact; $S = 0.98$, $P_{St} = 295$, $\varepsilon_B = 81$, $Re = 174$, $P_G(t = 0) = 24400$, $P_G(t = t_1) = 298$. Indicated dimensional times follow the recordings in Fig. 1a as close as possible.

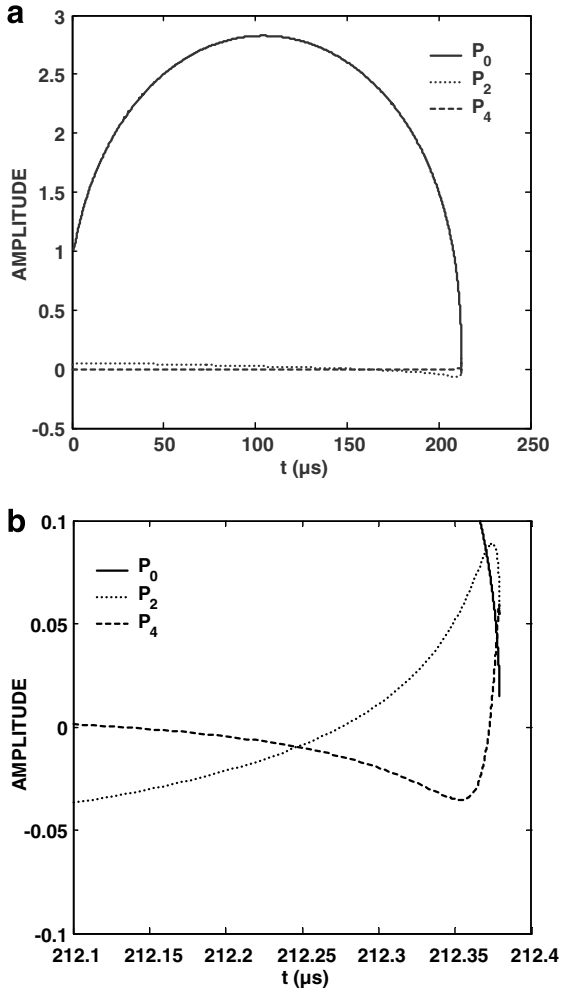

Fig. 4. Time variation of the zeroth, the second and the fourth Legendre modes of the bubble shape, for (a) the entire simulation and (b) the collapse phase, corresponding to Fig. 3.

accelerations that develop when the bubble acquires its minimum volume destabilize its shape giving rise to growth of higher modes, with P_2 being the dominant among them leading to jet formation and impact. In this process a tiny microbubble is formed at the center of the original bubble, Fig. 3c, surrounded by a larger toroidal bubble. In Fig. 5 the time evolution of the interfacial and jet velocities is monitored. The latter corresponds to the speed of the jet tip. The interfacial velocity is large enough to generate a shock wave, for both $S = 1$ and 0.98 as illustrated in Fig. 5a and b, an issue already discussed elsewhere [15]. The jet speed when $S = 0.98$, Fig. 5c, is smaller than the interfacial velocity when $S = 1$, nevertheless it is still quite large and focused locally around the jet tip. It should also be stressed that both velocities are overestimated owing to the absence of compressibility effects in the model. The latter is expected to damp the collapse process by mainly leading to smaller accelerations and, to a lesser extent, to larger minimum volume. Further research is required in order to get an exact estimate of the amount of damping due to compressibility effects, in the presence of shape deformation [15].

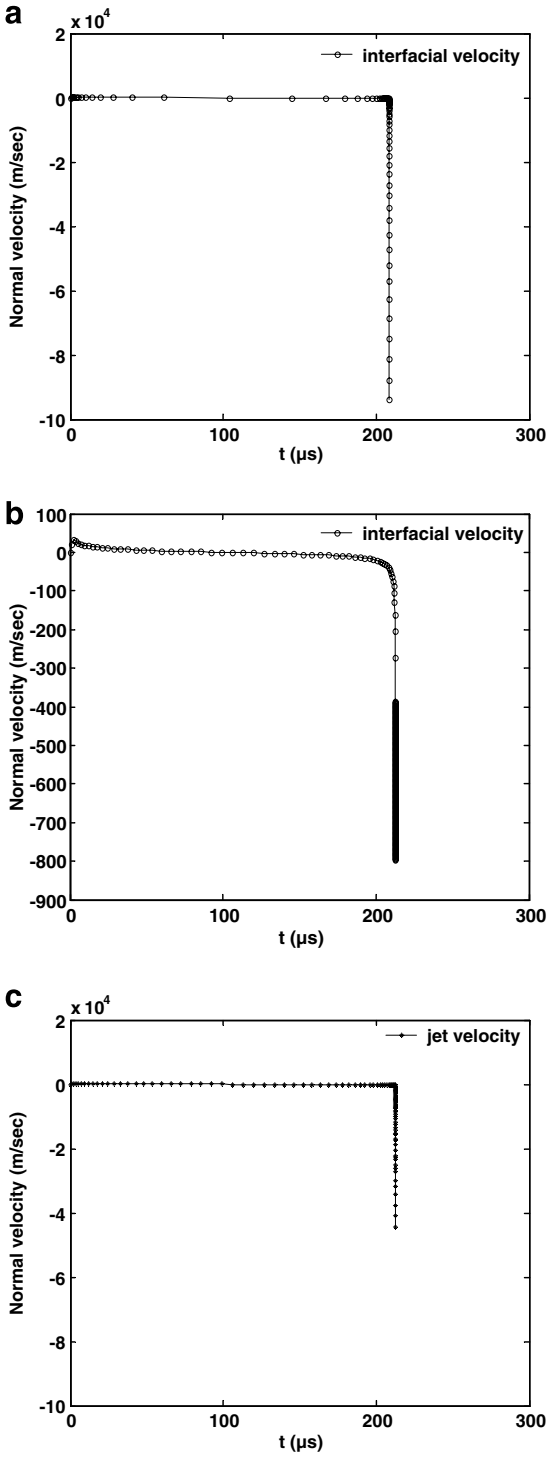

Fig. 5. Interfacial velocities for (a) $S = 1$, (b) $S = 0.98$ and jet velocity for (c) $S = 0.98$, during collapse of a nano-second bubble as shown in Figs. 2 and 3.

The same collapse pattern prevails for greater initial elongation until $S \approx 0.8$, in which case the bubble collapses via two jets that enter through its two poles, propagate in the opposite direction along the axis of symmetry, X-axis, and eventually coalesce in a centered fashion at the equatorial plane, the Y-axis, thus forming a tiny microbubble

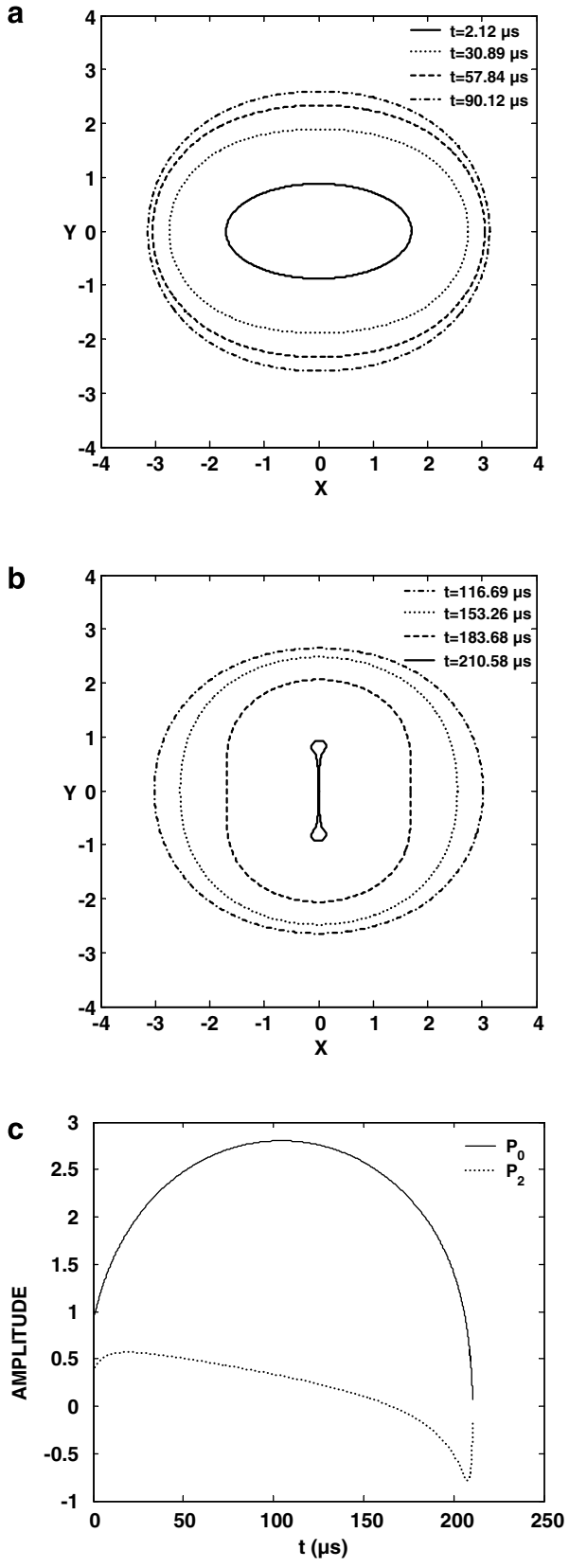

Fig. 6. Simulations of shape oscillations of nano-second laser bubbles in water during (a) bubble expansion and (b) bubble contraction and collapse. (c) Time variation of the zeroth and second Legendre modes of the bubble shape; $S = 0.8$, $P_{St} = 295$, $\varepsilon_B = 81$, $Re = 174$, $P_G(t = 0) = 24400$, $P_G(t = t_1) = 298$.

surrounded by a toroidal one; see also Fig. 6a and b. The pattern of jet motion, namely propagation along the axis of symmetry X or along the equator Y, depends on the phase of P_2 growth during which jet propagation and impact occurs. While the P_2 content of the bubble shape is negative jet propagation occurs along the X-axis and an oblate shape is obtained, Fig. 6b. Jet velocities obtained in this fashion are much smaller than those for the case with $S = 0.98$, hence they cannot instigate light emission upon impact. It is also worth mentioning that if the initial overpressure $P_G(t = 0_+)$ is increased beyond a critical value the collapse pattern shown in Fig. 3a–c is recovered with $S = 0.8$.

We also simulated the case of 5% water solution of acetone as host fluid with the appropriate thermophysical properties and a small initial elongation $S = 0.98$, but the sequence of bubble shapes that was obtained was very similar with those in Fig. 3, with pure water as the host liquid. This result can be attributed to the fact that the water has much higher vapor pressure than acetone and consequently the latter evaporates much easier. In addition, it was not easy to obtain the equilibrium radius of the bubble with great accuracy, based on the experiments, since the bubble had not fully stopped pulsating at the end of the recording. To obtain a shape sequence that is closer to the experimentally observed, Fig. 1b, it was necessary to reduce the pressure drop suffered by the bubble at $t = t_1$ in an effort to better simulate the process of recondensation taking place. The shape sequence shown in Fig. 7 was obtained in this fashion and exhibits a mild collapse that better conforms to experimental observations. Clearly a more rigorous account of the mass and heat transfer processes taking place inside the bubble during inception and collapse is needed if quantitative agreement with experimental results is required.

3. Simulation of single-bubble sonoluminescence (SBSL)

Acoustically levitated bubbles with equilibrium radius on the order of a few micrometers are trapped in the pressure antinode of a standing pressure wave due to the primary Bjerknes forces. Thus, they undergo radial oscillations at a more or less fixed position. Extensive experimental investigations have shown that the concentration of the dissolved gas and the temperature of the host liquid significantly affect the intensity of the emitted light, revealing the complexity of the phenomenon [10]. Furthermore, it has been established experimentally [11] that SBSL occurs under a narrow parameter range, in terms of sound amplitude and equilibrium radius, for given driving frequency and dissolved gas concentration. It is known [22] that for given dissolved gas concentration, relative to its saturation concentration, there is a threshold sound amplitude above which a bubble will grow due to rectified diffusion, whereas it will eventually dissolve below it. It was also shown [11] that there exists a small boundary line in the amplitude equilibrium radius plane (P_A, R_{Eq}) that separates regions

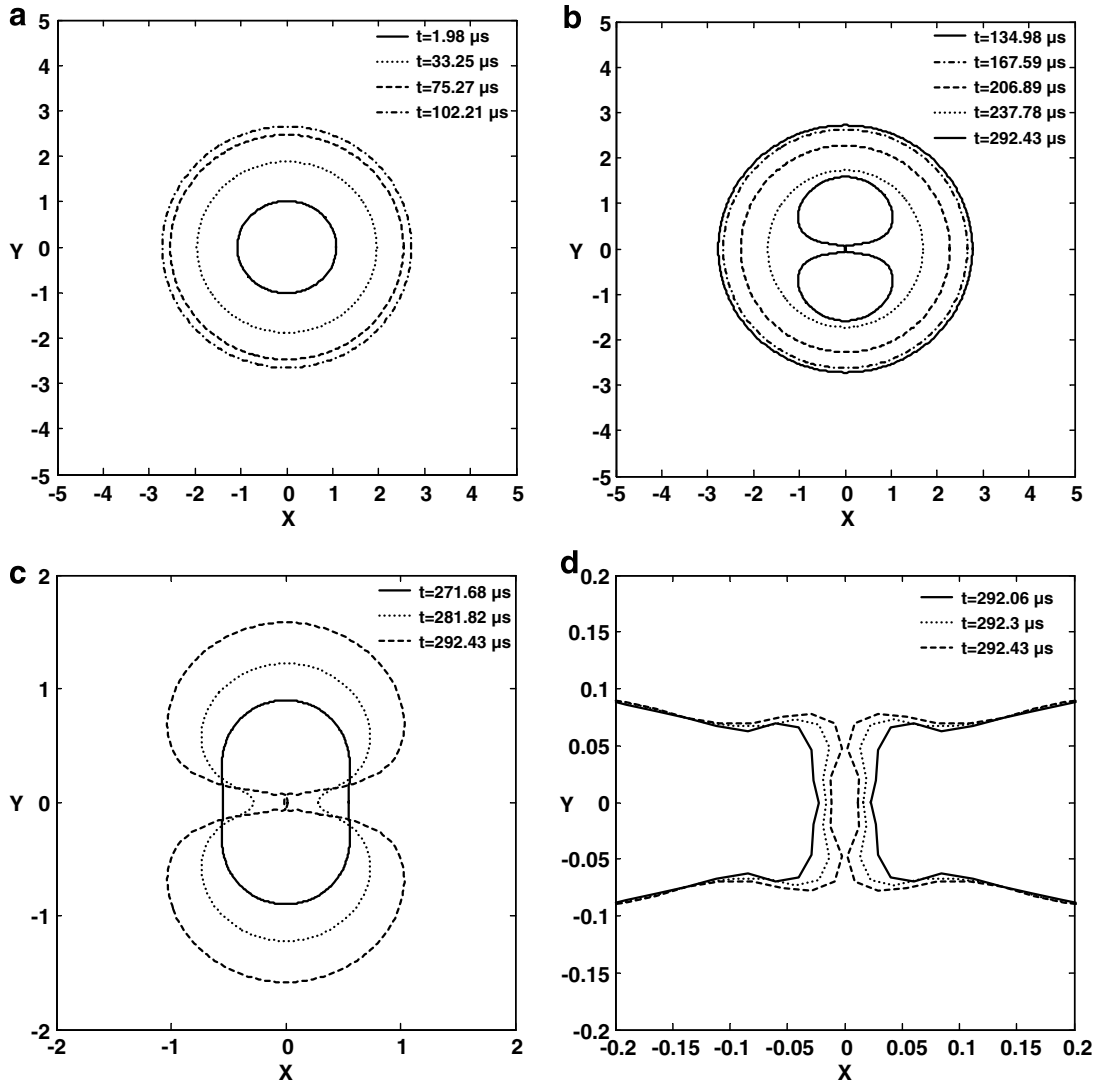

Fig. 7. Simulations of shape oscillations of nano-second laser bubbles in a 5% water solution of acetone (a) during bubble expansion, (b) during bubble contraction, (c) during rebound and jet impact and (d) focusing on jet impact; $S = 0.98$, $P_{St} = 302$, $\varepsilon_B = 30$, $Re = 176$, $P_G(t = 0) = 10000$, $P_G(t = t_1) = 1404$. Indicated dimensional times follow the recordings in Fig. 1b as close as possible.

of bubble growth and bubble dissolution as the bubble equilibrium radius R_{Eq} increases. This ensures the possibility for stable bubble pulsations, while shape instabilities and break-up prevail as P_A or R_{Eq} are further increased. This boundary line exists for parameter values over which sonoluminescence takes place [11]. Once rectified diffusion determines the bubble equilibrium size, then sound amplitude will determine the mechanics of collapse and subsequent light emission. Interestingly enough, stability analysis [14,15] reveals that in a similar parameter range shape instabilities set in and, in particular, transition from stable oscillations to parametric and Rayleigh–Taylor instability occurs. We are interested in simulating bubble collapse within the above parameter range in order to capture potential loss of spherosymmetry as well as the specific pattern of bubble deformation and break-up, in an effort to make some useful associations regarding the mechanism behind luminescence. In the literature of sonoluminescence [10,12,23] it is known that light emission is very sensitive to the amplitude of sound, dissolved gas concentration and heat capacity ratio, γ, but also to host liquid viscosity. We would like to investigate this sensitivity and, possibly, associate it with the collapse pattern. To this end, we employ the same numerical approach that was used for SCBL with the difference that in the case of SBSL a sinusoidal pressure wave is imposed on the far field pressure characterized by dimensionless amplitude ε and frequency v_f. In this case the dimensionless frequency constitutes an additional parameter, that is also made dimensionless via surface tension, $v_f = v'_f \cdot (\rho R_{Eq}^3/\sigma)^{1/2}$.

Experimental observations on SBSL in a water–glycerin mixture with high speed photography are available in the literature [4]. The photographic sequence of the experimentally obtained frames is reproduced in Fig. 8a and reveals that a trapped bubble of equilibrium radius $R = 8$ μm driven at 21.4 kHz carries out almost radial oscillations and

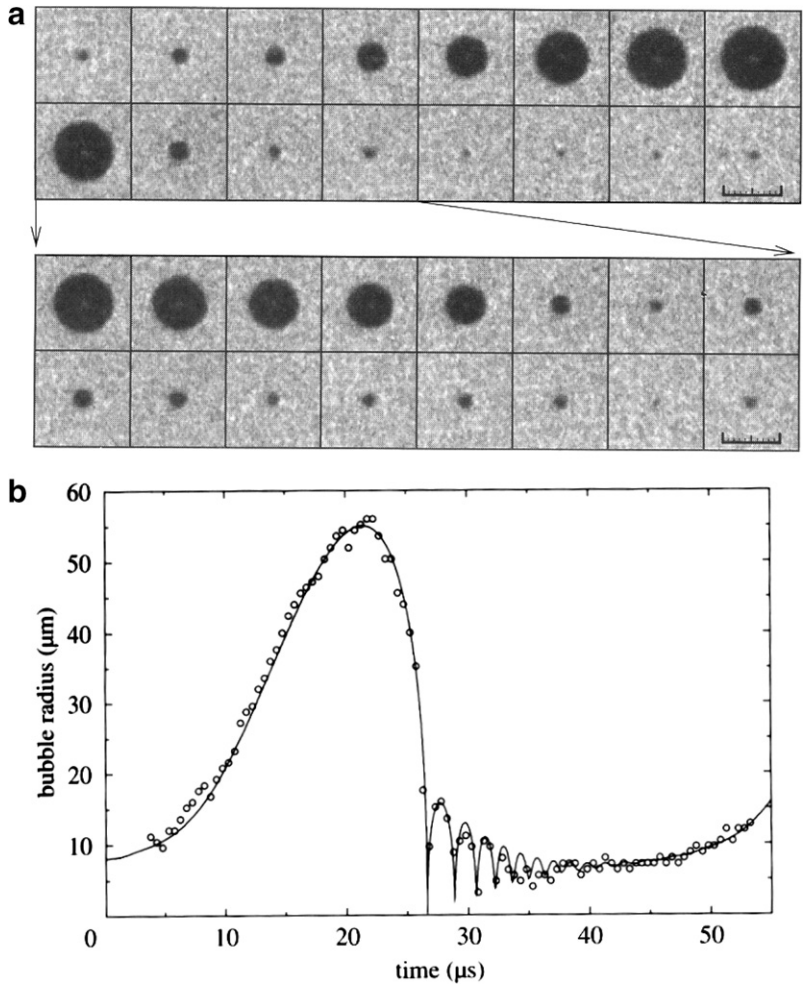

Fig. 8. (a) Photographic series of a trapped sonoluminescing bubble in a water–glycerin mixture driven at 21.4 kHz. The top row presents the bubble dynamics at an interframe time of ca. 2.5 μs. The bottom row shows the bubble collapse with five-fold temporal resolution (500 ns interframe time). The scale of image is indicated by the ruler (100 μm). (b) Radius–time curve from photographic observations. A numerically calculated curve is superimposed on the experimental data point (open circles). The calculation is based on the following parameters: driving frequency, $f_0 = 21.4$ kHz; ambient pressure, $p_0 = 1$ bar; driving pressure, $P_A = 1.32$ bar; vapor pressure, $p_v = 25$ mbar; equilibrium radius, $R_{Eq} = 8$ μm; density of the liquid, $\rho = 1000$ kg m^{-3}; viscosity, $\eta = 0.006$ N s m^{-2}; surface tension, $\sigma = 0.07$ N m^{-1}. The gas within the bubble is assumed to obey the adiabatic equation of state of an ideal gas with ratio of the specific heats of 1.33. All figures are reproduced from [4].

collapses in a more or less spherosymmetric fashion. This is true for all the stages of oscillation except, possibly, for the very last ones due to the extremely small size of the bubble. The experimental data for the time series of the bubble radius can be fitted to the Rayleigh–Plesset equation, Fig. 8b. The parameters obtained from the fitting, liquid viscosity in particular, can also be used in the present model in order to simulate bubble oscillation and collapse as close as possible. It must be stressed that due to the high viscosity of glycerin the resultant Reynolds number is $Re \approx 3.9$. The present axisymmetric model only takes into account weak viscous effects within the boundary layer of the bubble and this approach is accurate as long as Re remains large. In addition, the model does not account for the vapor pressure inside the bubble, which, however, is not expected to result in large discrepancies, and compressibility which is expected to increase the range of sound amplitudes before Rayleigh–Taylor instability destroys the bubble [24]. In order to overcome the above limitations we conducted a parametric study of the effect of different parameters on bubble collapse.

As a first test we simulated the case shown in Fig. 8 using the above mentioned parameter values, but assuming a small initial elongation characterized by $S = 0.96$. As it turns out, at the time instant at which the bubble acquires its minimum volume in the photographic sequence the simulations indicate collapse, Fig. 9a, along with the onset of jet formation. The signature of the latter effect is identified in Fig. 9b and c depicting the time evolution of the Legendre decomposition of the bubble shape throughout the simulation, Fig. 9b, and during collapse, Fig. 9c. The last figure shows rapid growth of almost all the harmonic components, P_2, P_4, P_6 and P_8. Linear stability analysis in the manner shown by Hilgenfeldt et al. [15] predicts very fast growth rate P_2 pertaining to a Rayleigh–Taylor instability. Towards the final collapse phase nonlinear energy transfer

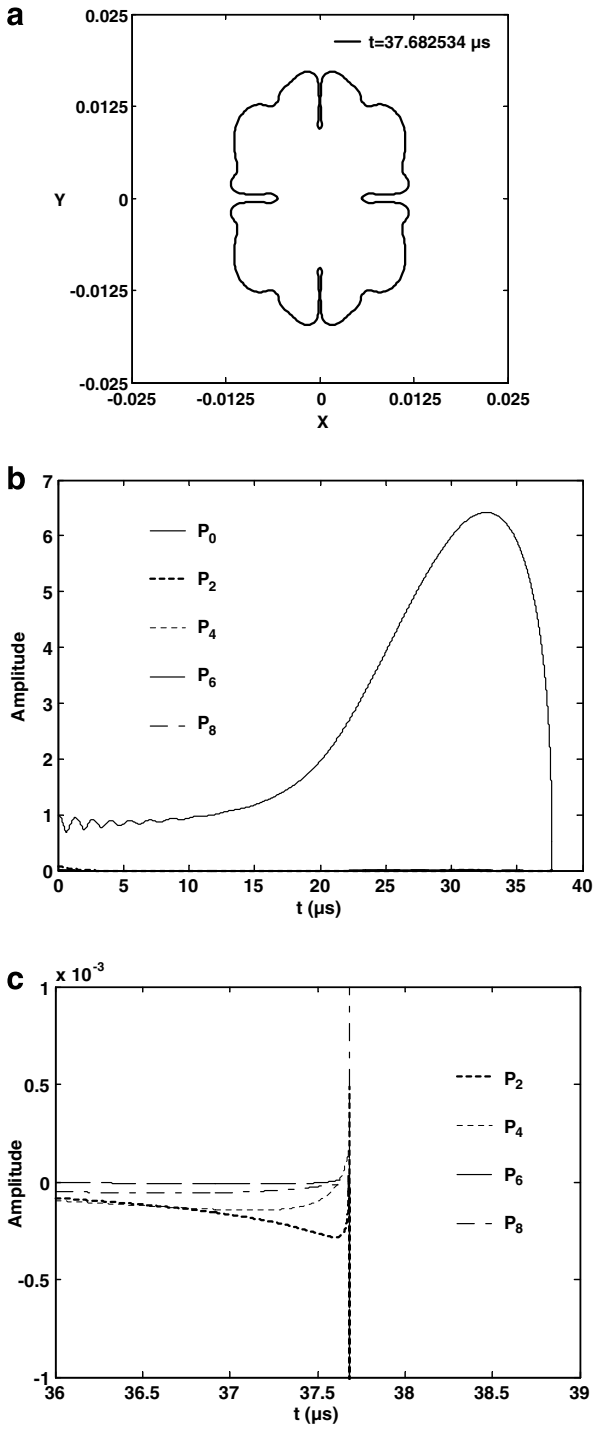

Fig. 9. (a) Interfacial shape at collapse of a single-bubble in a water–glycerin mixture. (b) Time variation of the first five even Legendre modes of the bubble shape during the entire simulation and (c) during collapse; $S = 0.96$, $P_{St} = 5.714$, $\varepsilon = 1.32$, $\omega_f = 0.364$, $Re = 3.9$.

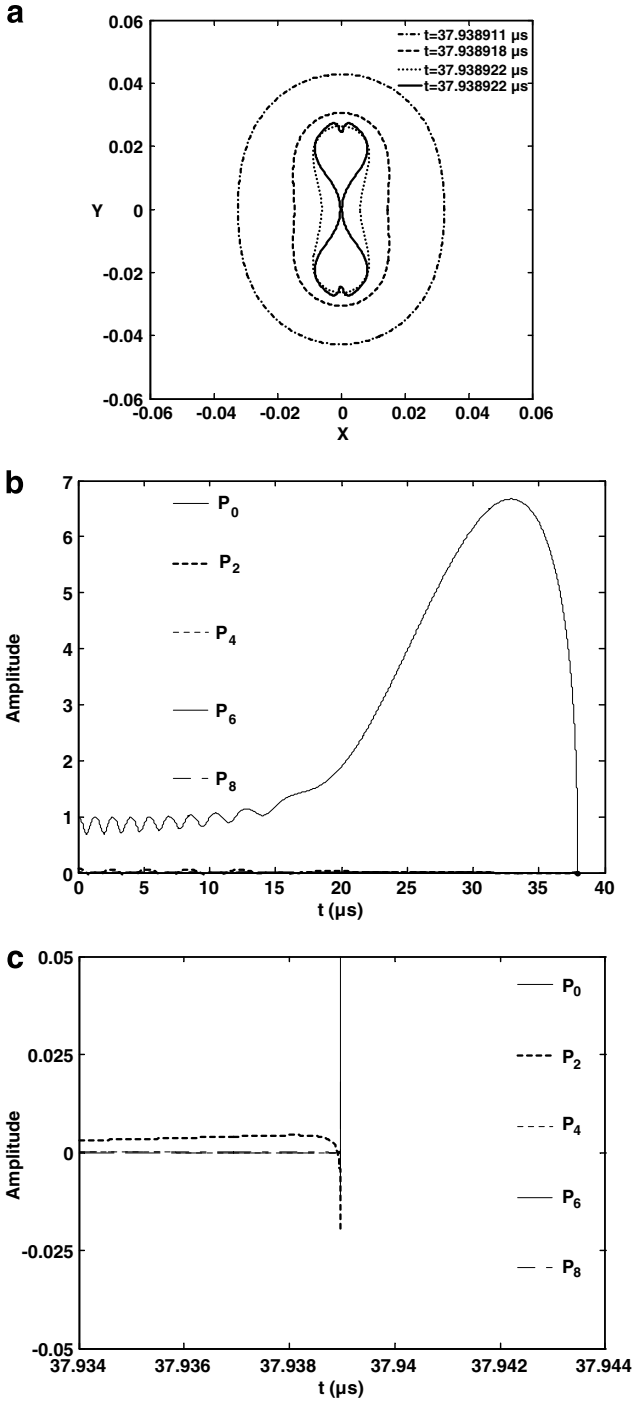

Fig. 10. (a) Interfacial shape during the collapse phase of a single-bubble in a water–glycerin mixture. (b) Time variation of the first five even Legendre modes of the bubble shape during the entire simulation and (c) during collapse; $S = 0.96$, $P_{St} = 5.714$, $\varepsilon = 1.32$, $\omega_f = 0.364$, $Re = 23.7$.

to even higher modes hinters further jet propagation and destroys the integrity of the bubble in regions of the interface where pinching occurs. Upon decreasing liquid viscosity to 0.001 N s/m^2, i.e. taking water as the host fluid, during the collapse phase the bubble exhibits jet formation and quick propagation along the axis of symmetry before impact, Fig. 10a. As can be gleaned from Fig. 10b and c, jet formation and impact is associated with rapid growth of the second Legendre shape mode. On comparing the situations depicted in Figs. 9 and 10, it turns out that viscosity does not significantly alter the minimum bubble volume or the Rayleigh–Taylor instability; see also Refs. [14,15]. However, it damps the explosive growth rate of P_2, which

might bear significance on the quenching of light emission in viscous fluids. Consequently, at large amplitudes and relatively small viscosities jet impact may occur before higher modes have the time to grow and pinch the bubble. It should also be noted that jet coalescence is accompanied by very large jet velocities at impact, Fig. 11b, attesting to the energy focusing nature of the phenomenon. The interfacial velocity is also shown in Fig. 11a, for the cases depicted in Figs. 9 and 10, corresponding to the radial velocity during the spherosymmetric part of the bubble collapse, which is also quite large and may produce a shock wave. The case with a higher *Re* leads to a lower velocity simply because jet impact occurs before Rayleigh–Taylor instability destroys the bubble. Then, the simulations have to stop. However, this is not the case with the bubble motion that may continue and lead to even higher velocities.

Jet formation and impact can be viewed as a manifestation of the afterbounce instability, and this is verified independently by linear stability analysis. Repeating the above simulations for a smaller amplitude, $\varepsilon = 1.1$, and water as the host fluid, jet propagation along the equator is obtained, Fig. 12a. The volume pulsation of the bubble clearly exhibits a sequence of afterbounces, Fig. 12b, signifying growth of P_2, Fig. 12c, and jet formation. The simulations stop due to jet impact while the P_2 content of the normal mode decomposition of the shape is positive, indicating a prolate shape. When the viscosity is increased to

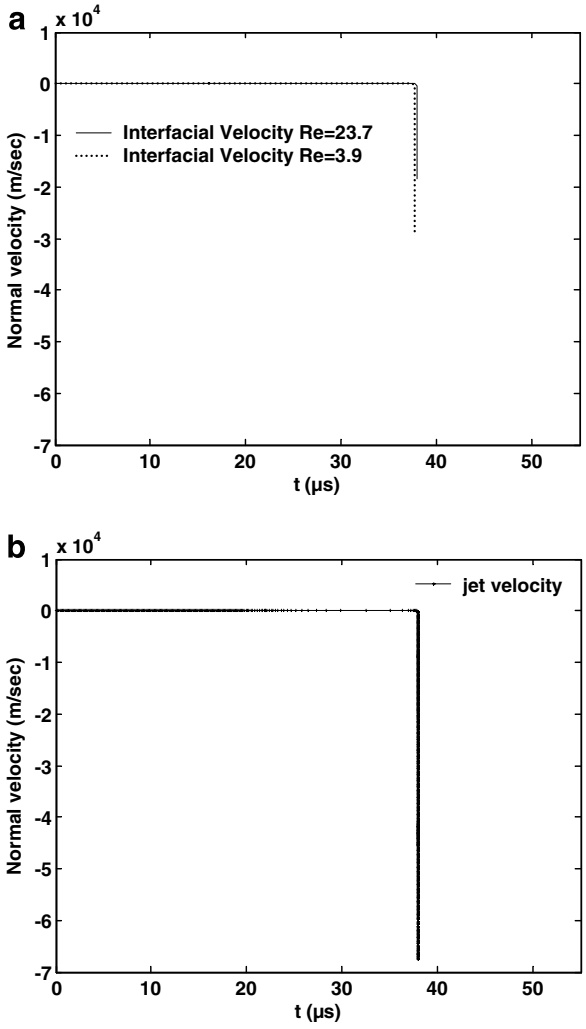

Fig. 11. (a) Interfacial velocity when $Re = 23.7$ and $Re = 3.9$ and (b) jet velocity during collapse when $Re = 23.7$; $S = 0.96$, $P_{St} = 5.714$, $\varepsilon = 1.32$, $\omega_f = 0.364$.

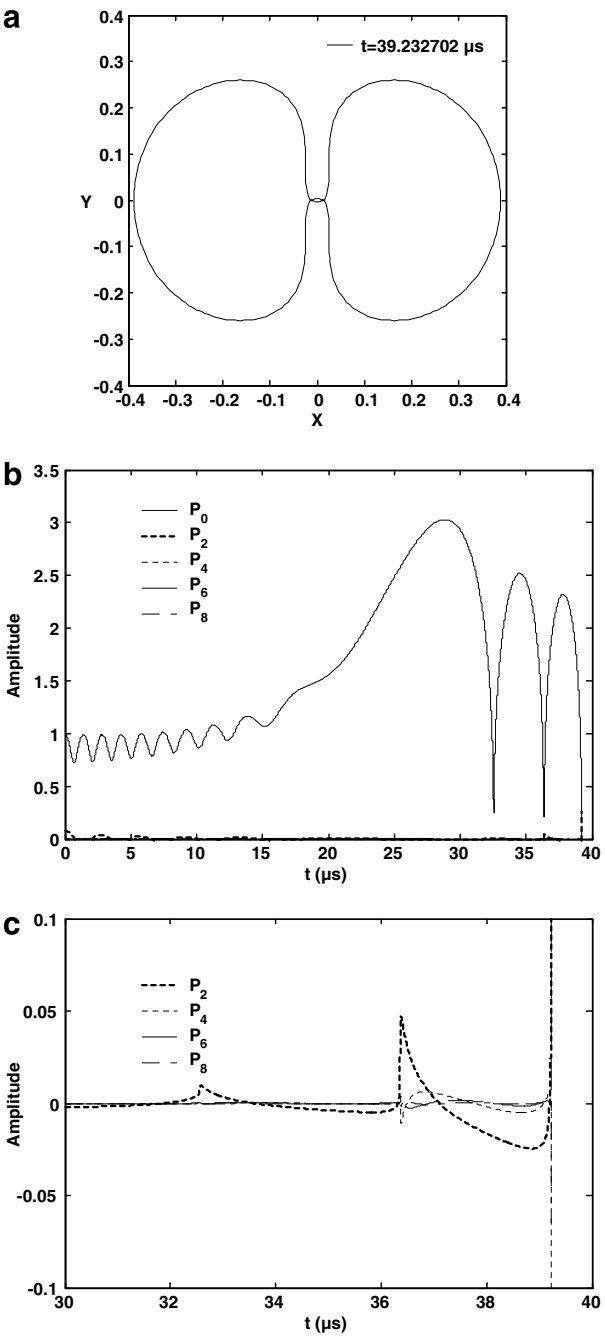

Fig. 12. (a) Interfacial shape at collapse of a single-bubble in water. (b) Time variation of the first five even Legendre modes of the bubble shape during the entire simulation and (c) during collapse; $S = 0.96$, $P_{St} = 5.714$, $\varepsilon = 1.1$, $\omega_f = 0.364$, $Re = 23.7$.

that of the water–glycerin mixture the volume afterbounces become weaker while P_2 growth is almost nonexistent. Similarly, further reduction of the disturbance amplitude below a certain threshold value, ε_{Cr}, for fixed liquid viscosity, eliminates jet impact; when $Re \approx 23.7$, $\varepsilon_{Cr} \approx 0.9$. Repeating the simulations with a smaller initial elongation, e.g. $S = 0.99$, does not change the collapse pattern at all except for the actual time of impact, Fig. 13, since anyway the initial P_2 content is damped before the onset of collapse. Even if a small amount of P_3 is introduced initially, still P_2 growth dominates the dynamics of collapse for most cases

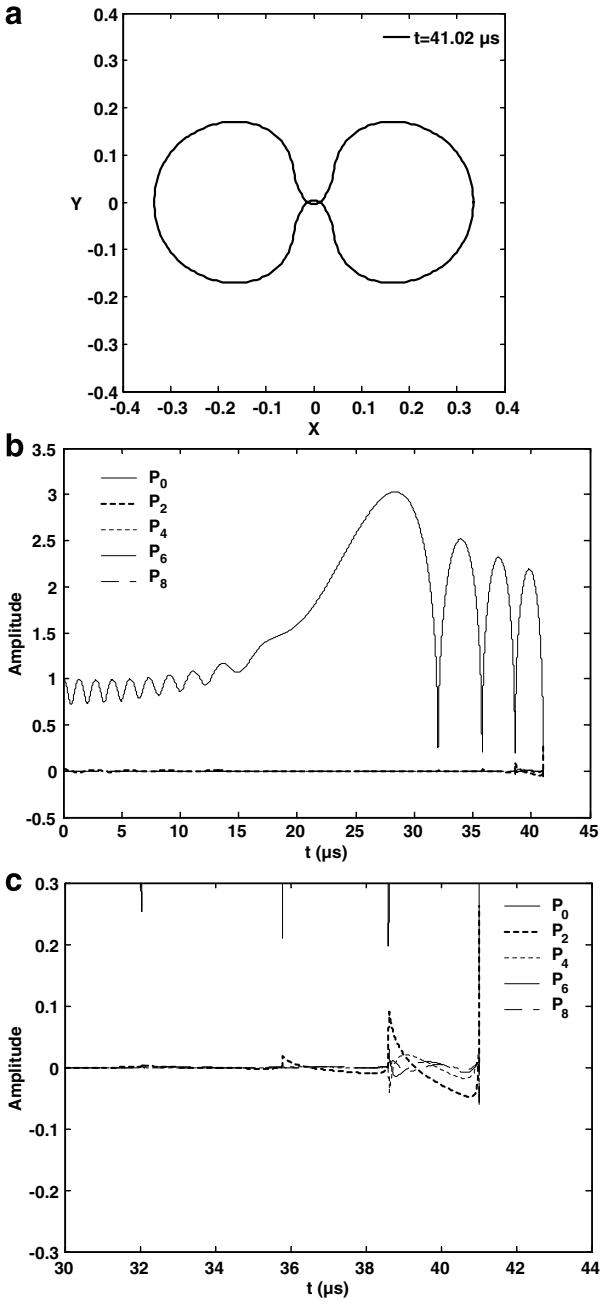

Fig. 13. (a) Interfacial shape at collapse of a single-bubble in water. (b) Time variation of the first five even Legendre modes of the bubble shape during the entire simulation and (c) during collapse; $S = 0.99$, $P_{St} = 5.714$, $\varepsilon = 1.1$, $\omega_r = 0.364$, $Re = 23.7$.

where an afterbounce instability is present. Jet formation and impact is associated with the major afterbounces following the collapse phase of the bubble. In fact, monitoring the amplitude ratio between the P_2 and P_0 pulsations it turns out that jet impact occurs when the magnitude of this ratio becomes on the order of 1. Performing linear stability analysis in the above parameter range verifies the pattern of P_2 growth or damping mentioned above.

It should be stressed that both here as well as with laser-induced bubbles, jet impact does not to necessarily destroy the integrity of the bubble. In fact, nano-second laser bubbles, as illustrated from the experimental observations shown in Fig. 1a, after acquiring their minimum volume they retract and eventually settle to their equilibrium radius. As shown from Fig. 2b, simulations indicate jet impact for this particular set of frames. If indeed this is the case, comparison between simulations and experiments with laser bubbles points in this direction, then jet impact may not destroy acoustically trapped bubbles either, but simply act as a dissipation mechanism of the excessive energy contained in the bubble during collapse. Unfortunately, our simulations have to stop once jet impact takes place. This is an interesting point that warrants further investigation, as it may be the case that jet formation and stable sonoluminescence coexist. Consequently, an acoustically trapped bubble may keep oscillating after impact and periodically exhibit the collapse-jet impact process. The energy associated with the process of jet impact is probably radiated away from the point of impact via secondary shock wave formation, while at the same time it is dissipated in order to heat the nearby gas and liquid masses.

When experimental observations, Fig. 8a and b, are compared against numerical results obtained using the actual mixture viscosity, Fig. 9, the latter indicate break-up via a Rayleigh–Taylor instability which precludes stable light emission. However, the present study does not account for the additional damping introduced by liquid compressibility. The latter is expected to affect the range of sound amplitudes over which afterbounce instability arises by translating it to higher ε values [18,24]. Carrying out linear stability analysis using the modified Rayleigh–Plesset equation that accounts for weak compressibility effects we obtain stability against P_2 growth for the parameter range that is relevant to the experimental observation shown in Fig. 8. Consequently, adiabatic collapse is probably the relevant mechanism for the flow arrangement in Fig. 8. However, jet impact and the energy focusing that it entails might provide a mechanism that will extend the range over which a collapsing bubble can emit light. This is an interesting issue that requires a more extensive numerical study, one that includes compressibility and heat transfer effects, in order to ascertain the range of jet impact and its possible association with light emission by acoustically trapped bubbles. Of course, this should be accompanied by a careful experimental investigation in the appropriate parameter range. It should also be stressed that when rapid penetration of liquid along the equatorial plane takes

place, instead of the axis of symmetry, the 3d topology of the flow is better described as "sink flow". It entails radial flow of a narrow liquid column towards the centre of the axis of symmetry. In order to convey the basic attributes of the 2d representation of the bubble shape at collapse, we retain the term jet for the two counter-propagating liquid columns that are shown to impact at each other in the respective 2d graphs, as a means to indicate the locality and intensity of the phenomenon.

4. Conclusions

In the present work we have simulated experiments on SCBL and SBSL after relaxing the assumption of spherosymmetry. The boundary integral method was used, which is capable of predicting the detailed axisymmetric deformation of the bubble interface during collapse, including weak viscous effects. Both for SCBL and SBSL, a small initial asphericity in the bubble shape is not clearly visible during the inception and expansion phases, however it may bear significant consequences during the collapse phase of the bubble, when the amplitude of the initial disturbance is large enough. In the case of SCBL, the initial asphericity of the bubble shape is produced at the early stages of bubble inception and varies from small to very large elongations. When the pulse duration is relative long, nano-second laser bubbles, large bubbles are generated, initial radius on the order of 0.5 mm, that clearly lose spherosymmetry at collapse, and this effect is captured by the simulations that also capture jet formation and impact. This is a result of an afterbounce instability arising during the collapse phase of the bubble and it is quite interesting if it is correlated with the fact that, according to the experiments, the bubble eventually retracts to its equilibrium indicating the stabilizing effect of impact.

In the case of SBSL the initial asphericity is very small and may only be due to very small variations in the primary Bjerknes force. Owing to the very small size of the bubbles, equilibrium radius on the order of 5 μm, loss of sphericity cannot be easily captured by high-speed photography. Nevertheless, in SBSL the volume pulsation is quite asymmetric, in comparison with SCBL, and consequently any initial elongation is mostly dissipated before the afterbounce instability sets in, compare Figs. 4 and 12, during the many afterbounces of the bubble volume after the major initial collapse. As a result initial elongation does not play a significant role in the simulations of acoustically trapped bubbles conducted here, aside from determining the exact time of impact. According to the simulations there is a narrow parameter window within which final collapse happens via jet impact that occurs, either through its two poles or through the opposite sides of the equatorial plane, with a very large velocity. It is a result of the afterbounce instability that leads to oblate or prolate shapes depending on the phase of P_2 growth that causes impact. As the amplitude further increases the collapse becomes more violent, jet formation is suppressed, and Rayleigh–Taylor instability prevails. As the amplitude decreases or the viscosity increases jet velocity during collapse decreases until jet impact is fully suppressed. It was also shown by the simulations that both the jet velocity, associated with the severity of jet impact, and bubble interfacial velocity, associated with the shock wave strength, are quite severe and may be correlated with light production. However, jet formation and impact was better captured by the simulations presented here, and it was seen in the context of experiments with laser induced bubbles that it does not necessarily lead to bubble fragmentation. It should then be investigated whether it can coexist with the process of continuous bubble pulsation in the context of SBSL, in which case it constitutes a mechanism that may extend the range of light emission predicted by adiabatic collapse.

Acknowledgements

Fruitful discussions with Dr. Reinhard Geisler and Dr. Robert Mettin, from the Drittes Physikalisches Institut Göttingen, regarding experiments with LASER induced nano-second and femto-second bubbles are gratefully acknowledged. The authors would also like to thank Dr. Reinhard Geisler and Pr. Werner Lauterborn for allowing reproduction of Fig. 1a and b and Fig. 7a and b from Dr. Geisler's Thesis and Ref. [4], respectively. Mr. Kostas Tsiglifis also wishes to acknowledge the HRAKLEITOS Program of the Greek Ministry of Education for financial support during this work.

References

[1] E. Heim, Uber das Zustandekommen der Sonolumineszenz, in: L. Cremer (Ed.), Proc. 3rd Int. Cong. on Acoustics, Stuttgart, 1959, Elsevier, Amsterdam, 1961, pp. 343–345.
[2] C.C. Wu, P.H. Roberts, A model of sonoluminescence, Proc. R. Soc. London A 445 (1994) 323–349.
[3] W.C. Moss, D.B. Clarke, D.A. Young, Calculated pulse widths and spectra of a single sonoluminescing bubble, Science 276 (1997) 1398–1401.
[4] C. Ohl, T. Kurz, R. Geisler, O. Lindau, W. Lauterborn, Bubble dynamics, shock waves and sonoluminescence, Philos. Trans. R. Soc. London A 357 (1999) 269–294.
[5] R. Geisler, Untersuchungen zur Laserinduzierten Kavitation mit Nanosekunden – Femtosekundenlasern, Ph.D. Thesis, submitted to the University of Goettingen, 2004.
[6] A. Prosperetti, A new mechanism for sonoluminescence, J. Acoust. Soc. Am. 101 (4) (1997) 2003–2007.
[7] T. Lepoint, D. De Pauw, F. Lepoint-Mullie, M. Goldman, A. Goldman, Sonoluminescence: an alternative 'electrohydrodynamic' hypothesis, J. Acoust. Soc. Am. 101 (4) (1997) 2012–2030.
[8] J.R. Blake, M.C. Hooton, P.B. Robinson, R.P. Tong, Collapsing cavities, toroidal bubbles and jet impact, Philos. Trans. R. Soc. London A 355 (1997) 537–550.
[9] H.N. Oguz, A. Prosperetti, Bubble entrainment by the impact of drops on liquid surfaces, J. Fluid Mech. 219 (1990) 143–179.
[10] B.P. Barber, C.C. Wu, R. Lofstedt, P.H. Roberts, S.J. Putterman, Sensitivity of sonoluminescence to experimental parameters, Phys. Rev. Lett. 72 (1994) 1380–1383.
[11] R.G. Holt, D.F. Gaitan, Observation of stability boundaries in the parameter space of single bubble sonoluminescence, Phys. Rev. Lett. 77 (18) (1996) 3791–3794.

[12] S. Hilgenfeldt, S. Grossmann, D. Lohse, Sonoluminescence light emission, Phys. Fluids 11 (6) (1999) 1318–1330.
[13] H.P. Brenner, S. Hilgenfeldt, D. Lohse, Single-bubble sonoluminescence, Rev. Mod. Phys. 74 (2) (2002) 425–484.
[14] M.P. Brenner, D. Lohse, T.F. Dupont, Bubble shape oscillations and the onset of sonoluminescence, Phys. Rev. Lett 75 (5) (1995) 954–957.
[15] S. Hilgenfeldt, D. Lohse, H.P. Brenner, Phase diagrams for sonoluminescing bubbles, Phys. Fluids 8 (11) (1996) 2608–2626, 9 2462(E).
[16] D.F. Gaitan, L.A. Crum, R.A. Roy, A.A. Church, Sonoluminescence and bubble dynamics for a single, stable cavitation bubble, J. Acoust. Soc. Am. 91 (1992) 3166.
[17] R. Toegel, S. Luther, D. Lohse, Viscosity destabilizes sonoluminescing bubbles, Phys. Rev. Lett. 96 (2006) 114301.
[18] H. Lin, B.D. Storey, A.J. Szeri, Rayleigh–Taylor instability of violently collapsing bubbles, Phys. Fluids 14 (8) (2002) 2925–2928.
[19] C.C. Wu, P.H. Roberts, Bubble shape instability and sonoluminescence, Phys. Lett. A 131–136 (1998) (1998).
[20] K. Tsiglifis, N. Pelekasis, Nonlinear oscillations and collapse of elongated bubbles subject to weak viscous effects, Phys. Fluids 17 (10) (2005) 1–18.
[21] K. Tsiglifis, N. Pelekasis, Non-linear oscillations and collapse of elongated bubbles subject to weak viscous effects: effect of internal overpressure, Phys. Fluids, submitted for publication.
[22] L.A. Crum, Measurements of the growth of air bubbles by rectified diffusion, J. Acoust. Soc. Am. 68 (1980) 203–211.
[23] R. Löfstedt, B.P. Barber, S.J. Putterman, Towards a hydrodynamic theory of sonoluminescence, Phys. Fluids A 5 (1993) 2911–2928.
[24] B.D. Storey, Shape stability of sonoluminescence bubbles: comparison of theory to experiments, Phys. Rev. E 64 (2001) 1–3, 017301.